

# Large-Area Chemically Modified Graphene Films: Electrophoretic Deposition and Characterization by Soft X-ray Absorption Spectroscopy

*By Vincent Lee,<sup>1§</sup> Luisa Whittaker,<sup>1§</sup> Cherno Jaye,<sup>2</sup> Kristen Baroudi,<sup>1</sup> Daniel A. Fischer,<sup>2</sup> and  
Sarbjit Banerjee<sup>1\*</sup>*

<sup>1</sup> Department of Chemistry, University at Buffalo, State University of New York, Buffalo, NY  
14260-3000; E-mail: sb244@buffalo.edu

<sup>2</sup> Materials Science and Engineering Laboratory, National Institute of Standards and  
Technology, Gaithersburg, MD 20899

*§ These authors contributed equally to this work*

## **Abstract**

A facile, rapid, and scalable electrophoretic deposition approach is developed for the fabrication of large-area chemically derived graphene films on conductive substrates based on the electrophoretic deposition of graphene oxide and reduced graphene oxide components. Two

distinctive approaches for fabricating conformal graphene films are developed. In the first approach, graphene oxide sheets are electrophoretically deposited from an aqueous solution after the oxidation of graphite to graphite oxide and the subsequent exfoliation of graphite oxide to graphene oxide. Next, the graphene oxide films are reduced via dip-coating in an aqueous solution of hydrazine. In the second approach, graphene oxide is reduced to graphene nanosheets in a strongly alkaline solution and the reduced graphene sheets are directly electrophoretically deposited onto conductive substrates. The film thickness can be modified by the deposition time and the obtained films span several square millimeters in area. Near-edge X-ray absorption fine structure (NEXAFS) spectroscopy is used to study the surface chemistry, electronic band structure, and degree of alignment of the electrophoretically deposited films.

## Introduction

Recent experimental progress in developing methods for fabricating strictly 2D crystals that were previously believed to be thermodynamically unstable have led to remarkable paradigm-shifting discoveries in solid state physics.<sup>1,2</sup> Graphene, a single layer of graphite, has attracted tremendous interest from the scientific community owing to its remarkable properties such as the room-temperature half-integer quantum Hall effect,<sup>3</sup> the massless Dirac fermion nature and extremely high mobilities of its charge carriers,<sup>4,5</sup> the tunability of its band gap (for graphene nanoribbons), and the potential for realizing ballistic conduction. Graphene also possesses fascinating thermal and mechanical properties,<sup>6</sup> which make it an attractive candidate for potential applications such as in electromechanical resonators,<sup>7</sup> stretchable and elastic matrices for flexible electronic circuitry,<sup>8</sup> stable field emitters,<sup>9,10</sup> ultracapacitors,<sup>11</sup> and as fillers for electrically conducting flexible nanocomposites.<sup>12</sup> The reliable fabrication of large-area graphene still remains a challenge although some progress has been achieved very recently using chemical vapor deposition and epitaxial growth methods.<sup>13,14</sup> Several approaches have been reported for obtaining single graphene sheets on substrates including the original micromechanical cleavage “scotch tape” method involving the repeated exfoliation of graphite mesas; however, this method gives a very low yield of typically sub-100  $\mu\text{m}$  graphene flakes masked by hundreds of thicker flakes of graphite and is thus unsuitable for precise positioning of graphene structures within device architectures and for scaling to practical quantities. Alternative approaches that have recently been reported include epitaxial growth on SiC<sup>15</sup> and the chemical vapor deposition of CH<sub>4</sub> over nickel catalysts.<sup>13</sup> Dai and co-workers have demonstrated very high mobilities for graphene nanoribbons with lateral dimensions <10 nm obtained by the chemical exfoliation of

commercial graphite using forming gas followed by surfactant-assisted dispersion in non-polar solvents. The obtained nanoribbons are semiconducting and exhibit on/off ratios as high as  $10^7$ .<sup>16</sup> Solution-chemistry-based approaches involving the initial oxidation of graphite to graphite oxide, followed subsequently by the mechanochemical or thermal exfoliation of graphite oxide to graphene oxide sheets, and their eventual reduction to graphene have also attracted much attention owing to the facile scalability and high yields obtained for these processes.<sup>8,12,17-21</sup>

Graphite oxide has been extensively studied over the last several decades and is known to have a much expanded interlayer separation as compared to crystalline graphite. In recent years, a broad consensus has emerged regarding the chemical structure of graphite oxide. The proposed structure places covalently bound epoxide (1,2-ether) and hydroxyl functional groups above and below the graphite basal planes with carboxylic acid groups thought to be located at edge sites.<sup>22</sup> The epoxide and hydroxyl groups are thought to be interspersed between intact conjugated domains. The presence of these functionalities decreases the van der Waals' interactions between adjacent graphitic layers and increases the interlayer separation to  $\sim 1.1$  nm from the 0.335 nm value observed for crystalline graphite, while also making the graphite oxide sheets electrically insulating. Furthermore, the polar functional groups facilitate dispersion of graphite oxide in water and other polar solvents, and the enhanced interlayer separation and diminished interlayer coupling enables the facile exfoliation of graphite oxide to single graphene oxide sheets upon thermal expansion or ultrasonication. The exfoliated graphene oxide sheets thus obtained can be subsequently chemically reduced to graphene sheets to substantially recover the desired electrical conductivity. Similar to pristine graphene, chemically derived graphene sheets have been shown to exhibit ambipolar behavior as a function of gate voltage, although the mobilities are about two orders of magnitude lower because of the persistence of lattice vacancies that are

not completely healed upon reduction with hydrazine or gaseous hydrogen.<sup>23</sup> The reduced graphene nanoplatelets are hydrophobic and are not amenable to dispersion in water. In the absence of other additives, these structures tend to agglomerate, forming poorly defined high-surface-area aggregates as electrostatic stabilization derived from polar functional groups is lost upon reduction.<sup>17</sup>

Several research groups have attempted to carefully reduce graphene oxide to graphene while still maintaining good dispersion of the graphene platelets in solvents with the goal of fabricating graphene thin films, membranes, and nanocomposites with tunable dimensions.<sup>17,20,21,24,25</sup> Achieving the optimal dispersion of graphene within polymers to form functional nanocomposites that reflect the desirable electrical and mechanical properties of the filler is critically dependent on the development of strategies to prevent the irreversible aggregation of graphene upon reduction. Towards this end, the reduction of graphite oxide sheets by hydrazine in the presence of poly(sodium 4-styrenesulfonate) (PSS) has been found to yield stable dispersions of graphene nanoplatelets<sup>26</sup> although the electrical properties of the resulting graphene sheets are likely compromised by the presence of the insulating polymer layer. The reduction of graphene oxide molecularly dispersed within polystyrene blends yields novel graphene-based nanocomposites with a percolation threshold of 0.1 vol% graphene for electrical conductivity.<sup>12</sup> Kaner and co-workers have spray-coated exfoliated graphene oxide platelets onto substrates and have proceeded to reduce these materials to graphene sheets using hydrazine. These authors report *p*-type semiconducting characteristics for field-effect transistor devices constructed using chemically derived graphene platelets as the active elements.<sup>24</sup> Chhowalla and co-workers have used a simple vacuum filtration technique to obtain ultrathin large-area flexible films of reduced graphene oxide exhibiting tunable sheet resistance and high optical

transparency.<sup>8</sup> One particularly elegant approach for stabilizing chemically reduced graphene nanoplatelets in solution without the addition of stabilizers or surfactants involves tailoring the electrostatic interactions between graphene platelets by careful control of the solution pH, graphene content, and electrolyte concentration.<sup>25</sup> This process involves increasing the solution pH by the addition of  $\text{NH}_3$  and the careful removal of metal ion species remnant from the graphite oxidation process, and is especially attractive owing to its yield of stable and processable graphene colloids without need for the addition of extraneous polymer or surfactant dispersants. Another simple and attractive approach for obtaining well dispersed reduced graphene oxide sheets has been reported by Ruoff, Nguyen, and co-workers and involves the reduction of exfoliated graphene oxide sheets in a strongly alkaline KOH/hydrazine aqueous solution.<sup>20</sup> The obtained reduced graphene sheets are also thought to be electrostatically stabilized, with the strongly alkaline pH inducing the ionization of the edge carboxylic acid groups and basal hydroxyl moieties. In another intriguing report, the deoxygenation of exfoliated graphene oxide to stable graphene dispersions has been noted under strongly alkaline conditions without the addition of strong reducing agents such as hydrazine.<sup>18</sup> These authors have claimed that the observed defunctionalization of graphene oxide under alkaline conditions mirrors the oxidation of graphite to graphite oxide under strongly acidic conditions.

Advances in dispersing and processing graphene such as the approaches outlined above have facilitated the fabrication of graphene films and free-standing graphene paper by methods such as spray-coating and vacuum filtration.<sup>8,21,24,25</sup> Nevertheless, the fabrication of large-area graphene coatings with tunable thicknesses on different substrates has not been exhaustively examined. We present here a facile and fully scalable electrophoretic deposition approach for the fabrication of smooth conformal films of graphene oxide and chemically derived graphene sheets

on conductive substrates. Two distinct approaches for fabricating chemically derived graphene films by electrophoretic deposition have been developed. In the first approach, exfoliated graphene oxide sheets are electrophoretically deposited onto an indium tin oxide (ITO)-coated glass substrate from aqueous solution and the resulting films are reduced by dipping in an aqueous solution of hydrazine hydrate. In the second approach, reduced graphene films are fabricated directly by electrophoretic deposition from an aqueous solution of reduced graphene platelets prepared by the hydrazine reduction of exfoliated graphene oxide in a strongly alkaline KOH solution. Conformal graphene films with good adhesion to underlying substrates prepared here are likely to be important building blocks for the fabrication of ultracapacitors, graphene-based field emitters, novel nanostructured anodes, and nanostructured coatings combining chemical stability, corrosion resistance, optical transparency, and electrical conductivity.

Despite the recent advances in processing chemically derived graphene nanoplatelets, considerable uncertainty still prevails regarding the electronic structure of these novel materials. Transport measurements indicate at least some degradation of electronic properties as compared to pristine graphene. Soft X-ray absorption spectroscopy based on the excitation of core electrons to empty or partially filled states is an excellent probe of the electronic band structure of graphite and related species such as carbon nanotubes.<sup>27-32</sup> However, only a very limited set of soft X-ray absorption spectroscopy experiments have been reported thus far for micromechanically cleaved graphene sheets<sup>33,34</sup> and no studies of chemically derived exfoliated graphene oxide or reduced graphene sheets have emerged thus far despite the clear need for these measurements to determine the effect of chemical processing on the graphene band structure above the Fermi level. We report here systematic angle-resolved near-edge X-ray absorption fine structure (NEXAFS) spectroscopy measurements of electrophoretically deposited graphene oxide and

graphene films. The dipole selection rules operational for NEXAFS spectroscopy yield detailed insight into the electronic band structure, surface chemistry, molecular orientation, and nature of alignment of the chemically derived graphene sheets in the electrophoretically deposited films.

## **Experimental**

*Preparation of graphite oxide and graphene oxide:* Graphite powders purchased from Qingdao Hensen Graphite Co. (China) with platelet sizes ranging from 150—300  $\mu\text{m}$  were used for the preparation of bulk graphite oxide. A modified version of Hummer's method<sup>35</sup> was used to oxidize graphite to graphite oxide. Briefly, 0.25 g of natural graphite powder and 0.125 g of  $\text{NaNO}_3$  were added to 5.75 mL of  $\text{H}_2\text{SO}_4$  under stirring in a flask that had been cooled to  $0^\circ\text{C}$  using an ice bath. Next, 0.75 g of  $\text{KMnO}_4$  was added slowly to the flask keeping the temperature below  $20^\circ\text{C}$ . Subsequently, the ice bath was removed and the flask was heated to  $35^\circ\text{C}$  and maintained at this temperature for 30 min, followed by the addition of 11.5 mL of deionized (DI) water. The temperature of the reaction mixture increased to  $\sim 98^\circ\text{C}$  upon the addition of water and the reaction vessel was maintained at this temperature for 15 min. Next, the suspension was further diluted with 34 mL of water and treated with 3%  $\text{H}_2\text{O}_2$  until the cessation of gas evolution. Finally, the suspension was vacuum filtered and left to dry under vacuum overnight after washing with copious amounts of DI  $\text{H}_2\text{O}$ . The solid graphite oxide thus obtained was then exfoliated in DI water by ultrasonication using a Ti tip sonicator (UP50H Hielscher Ultrasound Technology, power: 45 W; frequency: 30 kHz ) for 2 h to form a graphene oxide suspension with a concentration of  $\sim 1$  mg/mL. A homogeneous light yellow-brown solution was obtained after ultrasonication and was used for electrophoretic deposition without the addition of any additional "chargers".

*Preparation of reduced graphene dispersion:* An aqueous suspension of chemically modified graphene sheets was obtained using the KOH/hydrazine reduction protocol developed by Ruoff, Nguyen, and co-workers.<sup>20</sup> Potassium hydroxide was added to the exfoliated graphite oxide dispersion described above until the pH was between 10 and 11, and this solution was then stirred for 2 h before the addition of hydrazine hydrate. The hydrazine:graphene-oxide ratio was kept at 1:8. The reaction mixture was then stirred for 12 h at 35°C. Next, the resulting suspension was vacuum filtered through a fritted filter to remove large particles and the homogeneous filtrate comprising well-dispersed reduced graphene sheets was used for electrophoretic deposition. A control sample was also prepared by the reduction of graphene oxide by hydrazine without the addition of KOH.

*Electrophoretic deposition of graphene oxide and reduced graphene oxide films:* The exfoliated graphene oxide and reduced graphene oxide sheets were deposited onto ITO-coated glass electrodes (Delta Technologies, sheet resistance  $R_s = 5\text{--}10\ \Omega$ ; dimensions of 12.5 mm  $\times$  25 mm  $\times$  0.5 mm) using a home-built electrophoretic deposition setup. Briefly, a pair of ITO-coated glass electrodes with a separation of 2 mm was mounted onto glass slides with the conducting ITO sides facing each other to simulate a parallel-plate-like geometry. The entire electrode assembly was placed within the sample holder of a TL0.01 dip coater (MTI Corp.). Conducting leads were attached to the two ITO electrodes using Ag paste and the set of electrodes were slowly submerged into the appropriate graphene-oxide/reduced graphene oxide aqueous solution. Electrophoretic deposition was performed in constant current mode at DC currents of 0.1—1.0 mA using a Keithley 220 programmable current source. After electrophoretic deposition for 1—15 min, the graphene-coated films were withdrawn from the solutions at a rate of  $<0.3\ \text{mm}\ \text{min}^{-1}$  using the dip-coater.

*Characterization:* Differential scanning calorimetry (DSC, Q200, TA instruments) measurements under a flowing gaseous nitrogen atmosphere over a temperature range from -20 to 500°C were used to study the thermal behavior of graphite oxide and reduced graphite oxide. The  $\zeta$ -potentials of the exfoliated graphene oxide and reduced graphene oxide suspensions were measured using a Malvern Nano ZS90 instrument with irradiation from a 632.8 nm He-Ne laser. The chemically modified graphene solutions were filled in folded capillary cells and measured using a mixed mode method combining fast field and slow field reversal, which eliminated electroosmotic effects. The Smoluchowski approximation was used to determine the  $\zeta$ -potential of the graphene platelets from the electrophoretic mobility distribution for all the aqueous solutions studied here.

An Olympus BX41 optical microscope was used to obtain digital images of the surfaces of the electrophoretically deposited films. The morphologies and uniformity of the obtained films were also examined by scanning electron microscopy (SEM, JSM-5610LV) at an accelerating voltage of 20 kV. Raman spectra of the precursor graphite oxide and the deposited films were acquired using a Horiba Jobin Yvon Labram HR system with 514.5 nm laser excitation.

Carbon and oxygen K-edge NEXAFS measurements were performed at the National Institute of Standards and Technology (NIST) beamline U7A of the National Synchrotron Light Source at Brookhaven National Laboratory. A toroidal spherical grating monochromator with 600 lines/mm was used to acquire C K-edge data yielding an energy resolution of  $\sim 0.1$  eV, whereas a 1200 lines/mm grating was used to acquire O K-edge spectra with an energy resolution of  $\sim 0.15$  eV. NEXAFS spectra were collected in partial electron yield (PEY) mode with a channeltron electron multiplier detector near the sample surface using the detector with a -200 V entrance grid bias to enhance surface sensitivity. An electron charge compensation gun was used to

eliminate charging effects. To eliminate the effect of incident beam intensity fluctuations and beamline optics absorption features, the PEY signals were normalized using the incident beam intensity obtained from the photoemission yield of a freshly evaporated Au grid with 90% transmittance placed along the path of the incident X-rays. A standard metallic vanadium reference mesh was used for energy calibration of the O K-edge spectra and a carbon mesh was used for energy calibration of the C K-edge spectra using the  $\pi^*$  transition of graphite at 285.1 eV. Pre- and post-edge normalization of the data was performed using the Athena and Igor suite of programs.

## **Results and Discussion**

Surface charges on lyophobic colloidal particles not only serve to prevent their agglomeration but also provide a means for manipulating and positioning them in 3D space and on substrates by the application of electric fields. The electrophoretic deposition of nanomaterials from organic and aqueous solutions by the application of DC fields has emerged as an attractive scalable, rapid, and inexpensive route for the fabrication of nanostructured films.<sup>36-39</sup> We report here the deposition of exfoliated graphene oxide and chemically derived reduced graphene films on ITO substrates by the application of DC electric fields to aqueous suspensions of the appropriate nanomaterials.

Previous research has shown that graphite oxide can undergo complete exfoliation in water owing to the disruption of interlayer coupling upon functionalization, yielding a suspension of graphene oxide sheets that can be reduced or further chemically functionalized.<sup>17,20</sup> Graphene oxide sheets obtained by the ultrasonic exfoliation of graphite oxide yield a stable suspension in water because of electrostatic stabilization from polar and ionizable functional groups that impart

a negative charge.<sup>25</sup> Figure 1 shows a plot of the  $\zeta$ -potential distribution for exfoliated graphene oxide sheets in water indicating the strongly negative surface charge on these materials. The  $\zeta$ -potential distribution is centered around -36 mV. Consistent with ideas of electrostatically mediated colloidal stability for particles with  $\zeta$ -potentials above 30 mV or below -30 mV,<sup>25,40</sup> the graphene oxide sheets form a solution that is stable over several months. These solutions are light brown in color suggesting the partial disruption of the conjugated sp<sup>2</sup>-hybridized graphitic framework. Figure 1 also shows the  $\zeta$ -potential distribution of the KOH/hydrazine reduced graphene oxide sheets prepared using the method developed by Nguyen, Ruoff, and co-workers.<sup>20</sup> The reduction of graphene oxide by hydrazine in the presence of KOH yields dark solutions indicating significant recovery of the conjugated network. This approach for reducing graphene oxide is especially attractive because of the retention of the dispersion of the resulting chemically derived graphene nanoplatelets in water without the addition of surfactants or polymers. The  $\zeta$ -potential trace for this sample shows a very negative surface potential centered around -78 mV consistent with the increased ionization of species such as the carboxylic acid groups located at edge sites at high pH values. Notably, the hydrazine reduction protocol is expected to result in the deoxygenation of the epoxide species on the basal planes but is likely to leave the carboxylic acid groups at the edge sites intact, and thus the latter can help in electrostatically stabilizing the reduced graphene sheets at high pH.<sup>25</sup> Potassium ions likely associate with the charged carboxylic acid groups at the edge sites to form carboxylate ion pairs.<sup>20</sup> The conductivities of the graphene oxide solutions range from 0.1—0.5 mS/cm with the KOH solutions typically at the higher end of this range.

Smooth, conformal, and uniform films have been obtained on positive electrodes over large areas ranging up to several square millimeters based on the application of an electric field to

these graphene oxide suspensions as discussed in subsequent sections. As noted above, chemically derived graphene films have been prepared using two different approaches: a) reducing films fabricated by the electrophoretic deposition of graphene oxide by dip-coating in a hydrazine solution or b) the direct electrophoretic deposition of graphene nanosheets prepared by the KOH/hydrazine reduction of graphene oxide.

DSC traces have been obtained for exfoliated graphene oxide sheets and a control powder sample reduced by hydrazine. Figure 2A compares the DSC plots for the graphene oxide and reduced graphene oxide samples. The DSC curve of graphene oxide exhibits an exothermic peak at 230°C, which can be attributed to the removal of oxygenated groups (primarily epoxide and hydroxyl groups on the basal plane) to form water, whereas the hydrazine-reduced sample shows only an endothermic peak at 118 °C attributable to the removal of physically adsorbed water from the reduced graphene oxide surface; the latter feature is also present for the graphene oxide sample. The DSC data thus clearly evidences the efficacy of hydrazine in defunctionalizing graphene oxide. Figure 2B contrasts Raman spectra for graphene oxide and reduced graphene oxide powder samples. The spectra are characterized by two prominent peaks at 1340 and 1598  $\text{cm}^{-1}$ , which correspond to the *D* and *G* modes, respectively.<sup>41,42</sup> The *G* band corresponds to the first order scattering from the doubly degenerate  $E_{2g}$  phonon modes of graphite at the Brillouin zone center and is characteristic of all  $sp^2$ -hybridized carbon networks; the dispersive *D* band arises from phonon branches within the interior of the graphite Brillouin zone that are activated by scattering from defects;<sup>41,43</sup> the  $I_D/I_G$  ratio provides a sensitive measure of the disorder and crystallite size of the graphitic layers. Additionally, another prominent second-order dispersive feature, the *G'* band, is observed at  $\sim 2690 \text{ cm}^{-1}$  and is thought to originate from a two-phonon double resonance process. The prominent *D* band observed in Figure 2b for the graphite oxide

powder arises from the increased defect density upon functionalization of the graphitic basal planes with hydroxyl and epoxide groups. Remarkably, upon reduction with hydrazine, the  $I_D/I_G$  ratio very significantly decreases indicating considerable recovery of the conjugated graphitic framework upon defunctionalization of the epoxide and hydroxyl groups.

Figure 3 displays digital photographs, optical microscopy images, and scanning electron micrographs of graphene-based thin films prepared by the electrophoretic deposition of exfoliated graphene oxide and graphene oxide reduced by KOH/hydrazine onto ITO substrates. The graphene oxide films range in color from a light to a dark brown depending on the thickness; the brown color is consistent with the smaller size of intact conjugated domains within graphene oxide. In contrast, after reduction with KOH and hydrazine, the obtained reduced graphene oxide suspensions are black in color and yield darker films upon electrophoretic deposition. The films in Figure 3 have been found to range in thickness from 9.6 to 146 nm by spectroscopic ellipsometry measurements. We observe considerably smoother films upon deposition in constant-current mode as compared to deposition wherein the applied voltage is kept constant. The voltage applied during electrophoretic deposition is typically  $<20$  V. Spectroscopic ellipsometry results further indicate that the thickness of the films can be varied by adjusting the deposition time (1–20 min) although as observed with the electrophoretic deposition of other nanostructured materials, most of the functionalized graphene sheets are deposited within the first 5 min, likely corresponding to the deposition of the more extensively charged species that lie at the higher magnitude tails of the  $\zeta$ -potential distribution in Figure 1.<sup>38</sup> Film thicknesses ranging from 10–155 nm have been obtained and there appears to be a limiting thickness ( $<200$  nm) beyond which deposition does not proceed any further. Further increasing the applied DC voltage with the goal of increasing the film thickness results in turbulent flow and eventual

damage to the integrity of the deposited films from Joule heating effects. Notably, no extraneous chargers are added to the dispersions although the presence of some remnant metal ion species from the permanganate oxidation of graphite oxide can not be ruled out. Of course, reduced graphene oxide solutions prepared by the reduction of exfoliated graphene oxide by KOH and hydrazine have significant  $K^+$  ion concentration ( $K^+$  ions are also incorporated within the electrophoretically deposited films as discussed below) that enhance the conductivity of the solutions as noted above. The maximum thickness observed here is significantly less than the few micrometers typically obtained upon the electrophoretic deposition of other nanomaterials such as CdSe quantum dots or carbon nanotubes.<sup>36</sup> The optical microscopy and SEM images indicate the deposition of uniform films over large areas without evidence for any significant cracking. For thicker films some crumpling of the chemically derived graphene sheets is observed at the boundaries between individual graphene platelets as shown in Figure 3C for electrophoretically deposited graphene oxide films.

Figure 4 shows Raman spectra acquired for three films: a) an as-deposited graphene oxide film; b) the same film after reduction by dip-coating in an aqueous solution of hydrazine; and c) an as-deposited KOH/hydrazine-reduced graphene oxide film. The spectra have been normalized to the intensity of the *D* band. It is clear that hydrazine reduction results in a diminution of the *D*-band intensity (seen as an increase in the relative intensity of the *G* band), suggesting partial recovery of the conjugated graphene structure as noted above. Consistent with its darker color, the  $I_D/I_G$  intensity is the smallest for the KOH/hydrazine-reduced graphene oxide film, confirming substantial recovery of conjugated graphene domains. The difference between this film and the film reduced by dip coating in a hydrazine solution may also be that for the latter

film, reduction upon dip-coating in hydrazine solution occurs primarily for the surface layers and that the underlying layers remain substantially oxidized.

While electron microscopy provides some indication of the alignment and uniformity of the chemically derived graphene components within the electrophoretically deposited films, it is not a good probe of the local structure and alignment (local “flatness”) of the individual graphene components. Polarized NEXAFS spectroscopy provides detailed insight into the warping or alignment of the chemically derived graphene components of the films and thus a systematic angle-resolved NEXAFS study has been performed to simultaneously evaluate the electronic structure, surface chemistry, and degree of alignment of these nanostructured materials.<sup>27,32,33,44</sup> Figure 5 contrasts the C K-edge NEXAFS spectra acquired for the three films noted above at magic angle ( $54.7^\circ$ ) incidence where the peak intensities are expected to be independent of the angular asymmetry dependences of the transition matrix elements. C K-edge NEXAFS spectra correspond to the excitation of C 1s core electrons to unoccupied and partially filled levels in the conduction bands of graphitic systems, and thus to a good approximation reflect the unoccupied density of states (UDOS) above the Fermi level for these materials (as modified by core—hole effects). Band-theory-based descriptions of NEXAFS spectra with spectral features ascribed to transitions to all possible unoccupied one-electron states are in good agreement with electronic structure calculations for graphite and other extended  $sp^2$ -hybridized systems such as carbon nanotubes.<sup>27,32,33</sup> The lowest energy peak closest to the Fermi level at  $\sim 285.5$  eV (labeled as the  $\pi^*$  resonance in Fig. 5) can be attributed to transitions to states of  $\pi$  symmetry around the  $M$  and  $L$  points of the graphene Brillouin zone.<sup>27,32</sup> The sharply structured peak at  $\sim 292.55$  eV is thought to have some excitonic character<sup>34</sup> and arises from transitions to dispersionless unoccupied states possessing  $\sigma$  symmetry at the  $\Gamma$  point of the graphene Brillouin zone.<sup>27</sup> Of note

in the C K-edge spectra in Figure 5 is the increase in the intensity of the  $\pi^*$  resonance for the KOH/hydrazine reduced graphene films compared to the graphene oxide films before and after reduction, suggesting that the restoration of the  $sp^2$ -hybridized carbon network is better achieved by reduction prior to electrophoretic deposition. The higher energy features above 292.5 eV arise from higher lying conduction states of  $\pi$  and  $\sigma$  symmetry in the graphite/graphene DOS. Rosenberg et al. have qualitatively determined the symmetry of these states based on angle-resolved NEXAFS experiments of highly oriented pyrolytic graphite (HOPG) samples.<sup>27</sup> Notably, these features are significantly less defined in the graphene samples studied here as compared to HOPG samples,<sup>27</sup> consistent with the notion that even though interlayer coupling in graphite is fairly weak, the graphite band structure shows some clear differences from that of few layered graphene.<sup>33</sup> In other words, the reduced interlayer coupling in the electrophoretically deposited graphene films likely leads to the smearing and decrease in intensity of the higher energy features. Such behavior is also consistent with a multiple scattering view of NEXAFS spectra wherein the excited electron wave function is thought to be scattered by adjacent atoms. The lack of atoms in the immediate vicinity above and below the graphene basal plane due to increased interlayer separation thus reduces the cage of scattering atoms around the excited atom leading to a diminished intensity for these features. The KOH/hydrazine-reduced graphene sample shows two additional distinctive features at  $\sim 297.5$  and  $300.2$  eV arising from transitions to  $2p_{3/2}$  and  $2p_{1/2}$  states, respectively, at the K  $L$ -edge, indicating the incorporation of  $K^+$  ions in the electrophoretically deposited films.<sup>45,46</sup> The K  $L$ -edge peaks are shifted by  $\sim 3$  eV from literature values of 294.6 eV and 297.3 eV reported for potassium  $L$  edges.<sup>46</sup> Such shifts have been attributed to the formation of strongly ionic potassium—functional-group interactions<sup>45</sup> such as the potassium-ion—carboxylate bonds expected for the KOH/hydrazine-reduced

graphene samples. This observation confirms the formation of ion pairs upon reduction of graphene oxide by hydrazine in a strongly alkaline KOH solution. The graphene oxide film before reduction also shows two well-resolved spectral features at  $\sim 287.9$  and  $289.1$  eV between the  $\pi^*$  and  $\sigma^*$  resonances along with a shoulder at  $286.9$  eV. The  $289.1$  eV feature can be attributed to transitions to  $\pi^*$  C=O states derived from edge carboxylic acid groups based on previous studies of graphite oxide and molecular building blocks such as amino acids.<sup>34,47</sup> Indeed, Jeong et al. have attributed a feature at  $288.9$  eV in graphite oxide prepared by Brodie's method to such carboxylic acid moieties.<sup>34</sup> Analogously, the shoulder at  $\sim 286.9$  eV can be attributed to transitions from C 1s core levels to  $\pi^*$  C—OH states derived from basal phenolic groups of graphene oxide based on literature innershell absorption spectra of phenol, phthalic acid, and pyrocatechol.<sup>48</sup> The peak at  $\sim 287.9$  eV may represent a convolution of transitions to C—O states derived from epoxide moieties (a feature at  $\sim 287.2$  eV observed for graphite oxide has been thus attributed by Jeong et al.)<sup>34</sup> and intrinsic interlayer states in the conduction band of graphitic systems (a feature at  $\sim 288$  eV observed for graphene obtained by micromechanical cleavage has been thus attributed by Pacile et al.).<sup>32,33</sup> The latter is derived from a 3D conduction band feature with charge density predominantly concentrated between the basal planes and has been the subject of extensive theoretical and experimental study over the last two decades.<sup>32,49</sup> The interlayer states with free-electron character lie in the interior of the graphite/graphene Brillouin zone and have been shown to exhibit almost dispersionless behavior at the  $\Gamma$  point about  $5$  eV above the graphite Fermi level.<sup>32,33,49</sup> Such states are predicted to exist even for single-layered graphene, as has recently been demonstrated by Pacile et al. in photoemission electron microscopy (PEEM) experiments of micromechanically cleaved samples.<sup>33</sup> These states contain contributions from  $p_x$ ,  $p_y$ , and  $p_z$  orbitals and thus display neither  $\pi$  nor  $\sigma$  symmetry.

Notably, however we do not observe a shoulder to the  $\pi^*$  resonance at 283.7 eV proposed by these authors to be a characteristic signature of the UDOS of single and bilayered graphene. There are two likely reasons for the absence of this feature in our high-resolution C K-edge NEXAFS spectra. It is possible that the electrophoretically deposited films still have enough interlayer coupling to modify the electronic structure along the high-symmetry  $\overline{MK}$  direction so that transitions to characteristic graphene states are not observed. Notably, this feature is not observed even for few-layered graphene thicker than two graphene layers. Secondly, functionalization especially on the basal planes may also serve to sufficiently modify the band structure of graphene by disrupting the extended conjugated network. Detailed theoretical calculations are required to address the role of functionalization in modifying the electronic structure of graphene but based on the diminished mobilities observed in transport measurements perhaps it should not be surprising that chemically derived graphene differs at least in some subtle details of the band structure from pristine graphene. For the KOH/hydrazine reduced graphene films, the feature at 287.9 eV is far less prominent, consistent with the defunctionalization of epoxide and hydroxyl groups upon treatment with hydrazine;<sup>17</sup> in contrast, the 288.9 eV resonance ascribed to transitions to  $\pi^*$  C=O states derived from carboxylate moieties at edge sites is retained in all the samples, which agrees well with the reported inertness of  $-\text{COOH}$  groups to defunctionalization by hydrazine.<sup>17,25</sup>

Further evidence for the role of hydrazine in defunctionalizing the basal epoxide and hydroxyl groups of graphene oxide is provided by the O K-edge NEXAFS spectra shown in Figure 6. The spectra in this figure have only been pre-edge normalized to demonstrate the difference in the edge jump heights of the graphene oxide films before and after hydrazine reduction. The pre-edge normalized intensities beyond 550 eV are reflective of the relative oxygen concentrations in

the samples. Figure 6 clearly demonstrates the loss of oxygenated functional groups upon hydrazine reduction of the graphene oxide films. Two distinctive features are observed at the O K-edge: a weaker feature at  $\sim 531$  eV and a convolution of several peaks centered around 537 eV. The former can be ascribed to transitions from O 1s core levels to  $\pi^*$  C=O states derived from the carboxylic acid groups at the graphene oxide edge sites, as also noted in the C K-edge measurements.<sup>30,34</sup> The relatively lower intensity of this feature confirms the low abundance of carboxylic acid groups that are present only at edge sites. The higher energy components of the asymmetric and weakly structured feature centered at 537 eV observed for graphene oxide films both before and after reduction undoubtedly arise from transitions to O—H and C—O  $\sigma^*$  states derived from basal phenolic groups that have been reported at 535.4 and 539.7 eV, respectively, in O K-edge NEXAFS studies of graphite oxide.<sup>34</sup> The lower energy component of this broad asymmetric peak can be ascribed to transitions to antibonding C—O  $\sigma^*$  states derived from the abundant epoxide groups on the graphene oxide basal planes, consistent with the assignment of a 533.6 eV peak to epoxide species by Jeong et al for graphite oxide.<sup>34</sup> Remarkably, after hydrazine reduction, it is clearly apparent that the diminution in intensity at the O K-edge comes largely at the expense of the higher energy  $\sigma^*$  features and that the C=O  $\pi^*$  spectra feature originating from carboxylic acid groups at edge sites is largely unaffected, which further corroborates the role of hydrazine in reacting primarily with the epoxide and phenolic moieties on the graphene basal plane.<sup>17,25</sup>

Figure 7 shows polarized C K-edge NEXAFS spectra acquired for the electrophoretically deposited graphene oxide film prior to reduction. NEXAFS spectra not only reflect the UDOS of graphene as noted above but the transition matrix elements between the initial and final states are also incredibly sensitive to the polarization of the incident X-rays.<sup>31</sup> When the polarization vector

$\mathbf{E}$  is aligned along the bond axis, frontier orbital states with  $\sigma$  symmetry are probed, whereas when  $\mathbf{E}$  is perpendicular to the intermolecular bond axis, states with  $\pi$  symmetry are selectively observed. In other words, the NEXAFS dipole selection rules give rise to a “searchlight effect” wherein different partially filled or empty states above the Fermi level are observed depending on their symmetry and spatial orientation by varying the angle of incidence of the linearly polarized incident X-rays, thus making this technique an excellent probe of the anisotropy and bond orientation of different materials.<sup>31,50</sup> In recent work NEXAFS spectroscopy has been used to evidence the order and alignment of carbon nanotube arrays and films with considerable surface sensitivity.<sup>29,44</sup> The polarized NEXAFS spectra of the electrophoretically deposited graphene oxide films in Figure 7 clearly evidence considerable dichroism. At normal incidence ( $\theta = 90^\circ$ ),  $\mathbf{E}$  is in the plane of the electrophoretically deposited films and dipole selection rules only allow transitions to states with  $\sigma$  symmetry. Indeed, the  $\pi^*$  resonance at 285.45 eV is found to be significantly attenuated at normal incidence with the remnant intensity suggestive of some misalignment of graphene oxide nanoplatelets within the films and also perhaps the warping or 3D crumpling of individual graphene oxide sheets. Conversely, for  $30^\circ$  incidence of the linearly polarized X-rays,  $\mathbf{E}$  has a significant component perpendicular to the plane of the film (along the  $\pi$  cloud) and indeed the  $\pi^*$  resonance shows the strongest relative intensity with the  $\sigma^*$  resonance most attenuated in intensity at this angle. Figures 7B and C plot the integrated intensity of the  $\pi^*$  and  $\sigma^*$  resonances versus the angle of incidence. The assigned symmetries of the two resonances are further corroborated by the good fits to cosine-squared and sine-squared functions as shown in the figures.<sup>29,51</sup> Consistent with the assignment to  $\pi^*$  C=O states derived from carboxylic acid groups noted above, the 288.9 eV peak increases in intensity with decreasing angle of incidence, tracking the behavior of the graphitic  $\pi^*$  resonance. In contrast, the 287.8 eV feature thought to

be derived from interlayer states with additional contributions from epoxide moieties does not show a strong polarization dependence, which is consistent with the interlayer states possessing neither  $\sigma$  nor  $\pi$  symmetry.

It is useful to define a dichroic ratio (DR) as a quantitative measure of the extent of alignment of graphene sheets within the electrophoretically deposited films.

$$DR = \frac{(I_{\perp} - I_{\parallel})}{(I_{\perp} + I_{\parallel})} \quad (1)^{52}$$

where  $I_{\perp}$  is the integrated intensity of the  $\pi^*$  resonance at  $\theta = 90^{\circ}$  and  $I_{\parallel}$  is the extrapolate of the integrated intensity at  $\theta = 0^{\circ}$  obtained from the fitted cosine curves. A  $DR$  value of 0 is expected for a sample with completely random alignment of components (such as a completely amorphous polymer) and a  $DR$  value of -1 is expected for a perfectly aligned sample. A  $DR$  value of  $-0.45 \pm 0.08$  has been deduced for the graphene oxide film prior to reduction. As comparison, a freshly cleaved HOPG sample has been shown to have a  $DR$  value of -0.90, whereas freestanding carbon nanotube films (buckypaper) and vertically aligned carbon nanotube arrays have been shown to exhibit  $DR$  values ranging from -0.10 to +0.14 depending on their orientation with respect to the substrate. Thus, the as-deposited graphene oxide films clearly exhibit substantial alignment along the plane of the substrate.

Upon reduction with hydrazine, the dichroism evidenced in the C K-edge spectra marginally increases for the graphene oxide film. Figure 8 shows polarized NEXAFS spectra acquired for the graphene oxide film presented in Figure 7 after dip coating in a solution of hydrazine hydrate. Upon reduction, the  $\pi^*$   $DR$  increases in absolute value to  $-0.47 \pm 0.08$ , which suggests somewhat increased ordering at least at the surface of the reduced graphene oxide film. The restoration of conjugated graphene domains upon reduction likely leads to slightly better

stacking of graphene nanoplatelets within the electrophoretically deposited films yielding a slightly higher  $DR$  value. The removal of basal epoxide groups also likely paves the way for stronger  $\pi$ — $\pi$  interactions and the underlying layers can thus play a greater role in improving the stacking of graphene platelets.

Figure 9 shows polarized C K-edge NEXAFS spectra acquired for a reduced graphene film fabricated by the electrophoretic deposition of KOH/hydrazine-reduced graphene oxide. The darker color (Fig. 3B), decreased  $I_D/I_G$  band intensity observed in the Raman spectra (Fig. 4), and magic angle C K-edge data (Fig. 5) point to much greater restoration of the conjugated graphene domains upon reduction of graphene oxide prior to deposition. Consistent with these observations, Figure 9 clearly shows much greater dichroism in the C K-edge NEXAFS spectra as compared to the spectra for electrophoretically deposited graphene oxide or post-deposition-reduced graphene oxide films. The  $\pi^*$   $DR$  calculated for this film is  $-0.59 \pm 0.08$  corroborating that reduction in aqueous solution prior to deposition yields smoother and better aligned films as compared to the reduction of electrophoretically deposited graphene oxide films. Table 1 summarizes the dichroic ratios of the three films studied here. A likely scenario that emerges from this data is that graphene oxide reduced in strongly alkaline solutions retains extended conjugated  $sp^2$ -hybridized domains with carboxylic acid groups (and potassium-ion-carboxylate ion pairs) at edge sites enabling aqueous dispersibility as a result of electrostatic interactions. These largely intact and rigid domains are attracted by the electric field and travel to the electrodes where they transfer charge and are deposited on the electrode surface. The rigidity of the domains and ability to stabilize subsequent layers by  $\pi$ — $\pi$  interactions results in relatively less warping/crumpling of the deposited chemically derived graphene sheets. The remnant misalignment is likely at the interface between graphene sheets on the same plane.

In conclusion, we demonstrate a facile, fully scalable, and rapid method for the fabrication of large-area conformal graphene films on conductive substrates based on the electrophoretic deposition of chemically derived graphene oxide and reduced graphene oxide nanoplatelets onto conductive substrates. Polarized soft X-ray absorption spectroscopy measurements enable identification of surface functional groups, changes in the graphene band structure, and allow evaluation of the alignment and rigidity/warping of the graphene sheets within the deposited films. Reduction with hydrazine prior to electrophoretic deposition is observed to lead to smoother and better aligned films as compared to the post-deposition reduction of electrophoretically deposited graphene oxide films. The large-area conformal graphene films represent attractive candidates for ultracapacitors, field-emitting displays, and tunable coatings.

### **Acknowledgments**

The authors gratefully acknowledge startup funding from the University at Buffalo for support of this work. This work was also partially supported by an Interdisciplinary Research and Development Fund (IRDF) grant from the University at Buffalo. LW acknowledges the Fulbright Foundation for supporting her stay at the University at Buffalo. Certain commercial names are presented in this manuscript for purposes of illustration and do not constitute an endorsement by the National Institute of Standards and Technology.

**References**

- (1) Geim, A. K.; Novoselov, K. S. *Nat. Mater.* 2007, 6, 183.
- (2) Novoselov, K. S.; Jiang, D.; Schedin, F.; Booth, T. J.; Khotkevich, V. V.; Morozov, S. V.; Geim, A. K. *Proc. National Acad. Sci. (USA)* 2005, 102, 10451.
- (3) Novoselov, K. S.; Jiang, Z.; Zhang, Y.; Morozov, S. V.; Stormer, H. L.; Zeitler, U.; Maan, J. C.; Boebinger, G. S.; Kim, P.; Geim, A. K. *Science* 2007, 315, 1379.
- (4) Novoselov, K. S.; Geim, A. K.; Morozov, S. V.; Jiang, D.; Katnelson, M. I.; Grigorieva, I. V.; Dubonos, S. V.; Firsov, A. A. *Nature* 2005, 438, 197.
- (5) Novoselov, K. S.; Geim, A. K.; Morozov, S. V.; Jiang, D.; Zhang, Y.; Dubonos, S. V.; Grigorieva, I. V.; Firsov, A. A. *Science* 2004, 306, 666.
- (6) Lee, C. E.; Wei, X.; Kysar, J. W.; Hone, J. *Science* 2008, 321, 385.
- (7) Bunch, J. S.; van der Zande, A. M.; Verbridge, S. S.; Frank, I. W.; Tanenbum, D. M.; M., P. J.; Craighead, H. G.; McEuen, P. L. *Science* 2007, 315, 490.
- (8) Eda, G.; Fanchini, G.; Chhowalla, M. *Nat. Nanotechnol.* 2008, 3, 270.
- (9) Eda, G.; Unalan, H. E.; Rupesinghe, N.; Amaratunga, G. A.; Chhowalla, M. *Appl. Phys. Lett.* 2008, 93, 233502/1.
- (10) Wu, Z.-S.; Pei, S.; Ren, W.; Tang, D.; Gao, L.; Liu, B.; Li, F.; Liu, C.; Cheng, H. M. *Adv. Mater.* 2009, 21, 1.

- (11) Stoller, M. D.; Park, S.; Zhu, Y.; Ruoff, R. S. *Nano Lett.* 2008, 8, 3498.
- (12) Stankovich, S.; Dikin, D. A.; Dommett, G. H. B.; Kohlhaas, K. M.; Zomney, E. J.; Stach, E. A.; Piner, R. D.; Nguyen, S. T.; Ruoff, R. S. *Nature* 2006, 442, 282.
- (13) Kim, K. S.; Zhao, Y.; Jang, H.; Lee, S. Y.; Kim, J. M.; Kim, k. S.; Ahn, J.-H.; Kim, P.; Choi, J.-Y.; Hong, B. H. *Nature* 2009, 457, 706.
- (14) Sutter, P. W.; Flege, J.-I.; Sutter, E. A. *Nat. Mater.* 2008, 7, 406.
- (15) Ohta, T.; Bostwick, A.; Seyller, T.; Horn, K.; Rotenberg, E. *Science* 2006, 313, 951.
- (16) Li, X.; Wang, X.; Zhang, L.; Lee, S.; Dai, H. *Science* 2008, 319, 1229.
- (17) Stankovich, S.; Dikin, D. A.; Piner, R. D.; Kohlhaas, K. M.; Kleinhammes, A.; Jia, Y.; Wu, Y.; Nguyen, S. T.; Ruoff, R. S. *Carbon* 2007, 45, 1558.
- (18) Fan, X.; Peng, W.; Li, Y.; Li, X.; Wang, S. C.; Zhang, G.; Zhang, F. *Adv. Mater.* 2008, 20, 4490.
- (19) McAllister, M. J.; Li, J.-L.; Adamson, D. H.; Schniepp, H. C.; Abdala, A. A.; Liu, J.; Herrera-Alonso, M.; Milius, D. L.; Car, R.; Prud'homme, R. K.; Aksay, I. A. *Chem. Mater.* 2007, 19, 4396.
- (20) Park, S.; An, J.; Piner, R. D.; Jung, I.; Yang, D.; Velamakanni, A.; Nguyen, S. T.; Ruoff, R. S. *Chem. Mater.* 2008, 20, 6592.
- (21) Dikin, D. A.; Stankovich, S.; Zimney, E. J.; Piner, R. D.; Dommett, G. H. B.; Evmenko, G.; Nguyen, S. T.; Ruoff, R. S. *Nature* 2007, 448, 457.

- (22) Lerf, A.; He, H.; Forster, M.; Klinowski, J. *J. Phys. Chem. B* 1998, *102*, 4477.
- (23) Gomez-Navarro, C.; Weitz, R. T.; Bittner, A. M.; Scolari, M.; Mews, A.; Burghard, M.; Kern, K. *Nano Lett.* 2007, *7*, 3499.
- (24) Gilje, S.; Han, S.; Wang, M.; Wang, K. L.; Kaner, R. B. *Nano Lett.* 2007, *7*, 3394.
- (25) Li, D.; Muller, M. B.; Gilje, S.; Kaner, R. B.; Wallace, G. G. *Nat. Nanotechnol.* 2008, *3*.
- (26) Stankovich, S.; Piner, R. D.; Chen, X.; Wu, N.; Nguyen, S. T.; Ruoff, R. S. *J. Mater. Chem.* 2006, *16*, 155.
- (27) Rosenberg, R. A.; Love, P. J.; Rehn, V. *Phys. Rev. B* 1986, *33*, 4034.
- (28) Comelli, G.; Stohr, J.; Jark, W.; Pate, B. B. *Phys. Rev. B* 1988, *37*, 4383.
- (29) Banerjee, S.; Hemraj-Benny, T.; Sambasivan, S.; Fischer, D. A.; Misewich, J. A.; Wong, S. S. *J. Phys. Chem. B* 2005, *109*, 8489.
- (30) Banerjee, S.; Hemraj-Benny, T.; Balasubramanian, M.; Fischer, D. A.; Misewich, J. A.; Banerjee, S. *Chem. Commun.* 2004.
- (31) Stohr, J. *NEXAFS Spectroscopy*; Springer: Berlin, 1992.
- (32) Fischer, D. A.; Wentzcovich, R. M.; Carr, R. G.; Continenza, A.; Freeman, A. J. *Phys. Rev. B* 1991, *44*, 1427.
- (33) Pacile, D.; Papagno, M.; Rodriguez, A. F.; Grioni, M.; Papagno, L.; Girit, C. O.; Meyer, J. C.; Begtrup, G. E.; Zettl, A. *Phys. Rev. Lett.* 2008, *101*, 066806/1.

- (34) Jeong, H.-K.; Noh, H.-J.; Kim, J.-Y.; Jin, M. H.; Park, C. Y.; Lee, Y. H. *EPL* 2008, 82, 67004/1.
- (35) Hummers, W. S. *J. Am. Chem. Soc.* 1958, 80, 1339.
- (36) Islam, M. A.; Herman, I. P. *Appl. Phys. Lett.* 2002, 80, 3823.
- (37) Mahajan, S. V.; Hasan, S. A.; Cho, J.; Shaffer, M. S. P.; Boccaccini, A. R.; Dickerson, J. A. *Nanotechnology* 2008, 19, 195301/1.
- (38) Jia, S.; Banerjee, S.; Herman, I. P. *J. Phys. Chem. C* 2008, 112, 162.
- (39) Patel, M. N.; Williams, R. D.; May, R. A.; Uchida, H.; Stevenson, K. J.; Johnston, K. P. *Chem. Mater.* 2008, 20, 6029.
- (40) Everett, D. H. *Basic Principles of Colloid Science*; The Royal Society of Chemistry: London, 1988.
- (41) Pimenta, M. A.; Dresselhaus, G.; Dresselhaus, M. S.; Cancado, L. G.; Jorio, A.; Saito, R. *Phys. Chem. Chem. Phys.* 2007, 9, 1276.
- (42) Dresselhaus, M. S.; Dresselhaus, G.; Hoffmann, M. *Philos. Trans. R. Soc. A* 2008, 366, 231.
- (43) Ferrarri, A. C.; Robertson, J. *Phys. Rev. B* 2000, 61, 14095.
- (44) Hemraj-Benny, T.; Banerjee, S.; Sambasivan, S.; Balasubramanian, M.; Fischer, D. A.; Eres, G.; Poretzky, A. A.; Geoghan, D. B.; Lowndes, D. H.; Han, W. Q.; Misewich, J. A.; Wong, S. S. *Small* 2006, 2, 26.

- (45) Richter, C.; Jaye, C.; Panaitescu, E.; Fischer, D. A.; Lewis, L. H.; Willey, R. J.; Menon, L. *J. Mater. Chem.* 2009, *19*, 2963.
- (46) Nelson, A. J.; van Buuren, T.; Miller, E.; Land, T. A.; Bostedt, C.; Franco, N.; Whitman, P. K.; Baisden, P. A.; Terminello, L. J.; Callcott, T. A. *J. Electron. Spectrosc. Relatd. Phenom.* 2001, *114-116*, 873.
- (47) Kaznachejev, K.; Osanna, A.; Jacobsen, C.; Plashkevych, O.; Vahtras, O.; Agren, H.; Carravetta, V.; Hitchcock, A. P. *J. Phys. Chem. A* 2002, *106*, 3153.
- (48) Francis, J. T.; Hitchcock, A. P. *J. Phys. Chem.* 1992, *1992*.
- (49) Strocov, V. N.; Blaha, P.; Starnberg, H. I.; Rohlfing, M.; Claessen, R.; Debever, J.-M.; Themlin, J.-M. *Phys. Rev. B* 2000, *61*, 4994.
- (50) Velazquez, J. M.; Jaye, C.; Fischer, D. A.; Banerjee, S. *J. Phys. Chem. C* 2009, *113*, 7639.
- (51) Sakai, T.; Ishikawa, K.; Takezoe, H.; Matsuie, N.; Yamamoto, Y.; Ishii, H.; Ouchi, Y.; Oji, H.; Seki, K. *J. Phys. Chem. B* 2001, *105*, 9191.
- (52) Smith, A. P.; Ade, H. *Appl. Phys. Lett.* 1996, *69*, 3833.

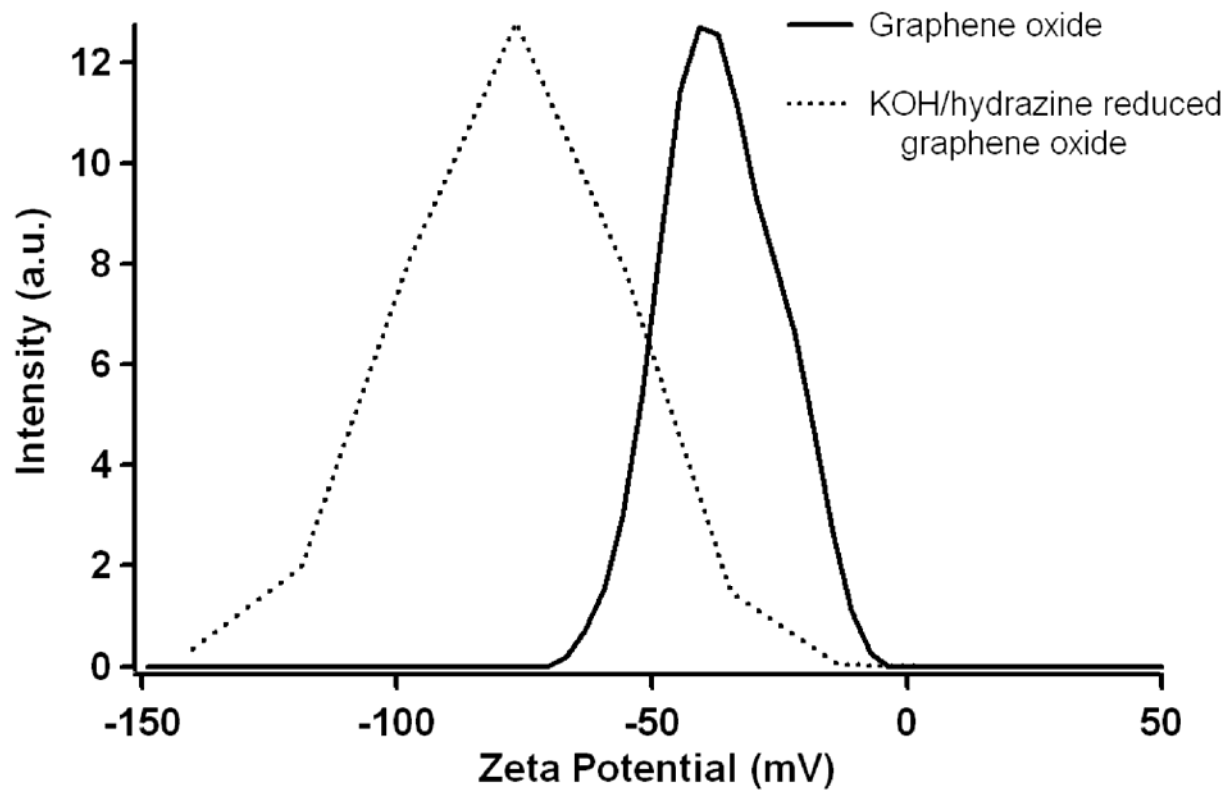


**Figure 1.**  $\zeta$ -potential distribution of graphene oxide and KOH/hydrazine-reduced graphene oxide sheets dissolved in water.

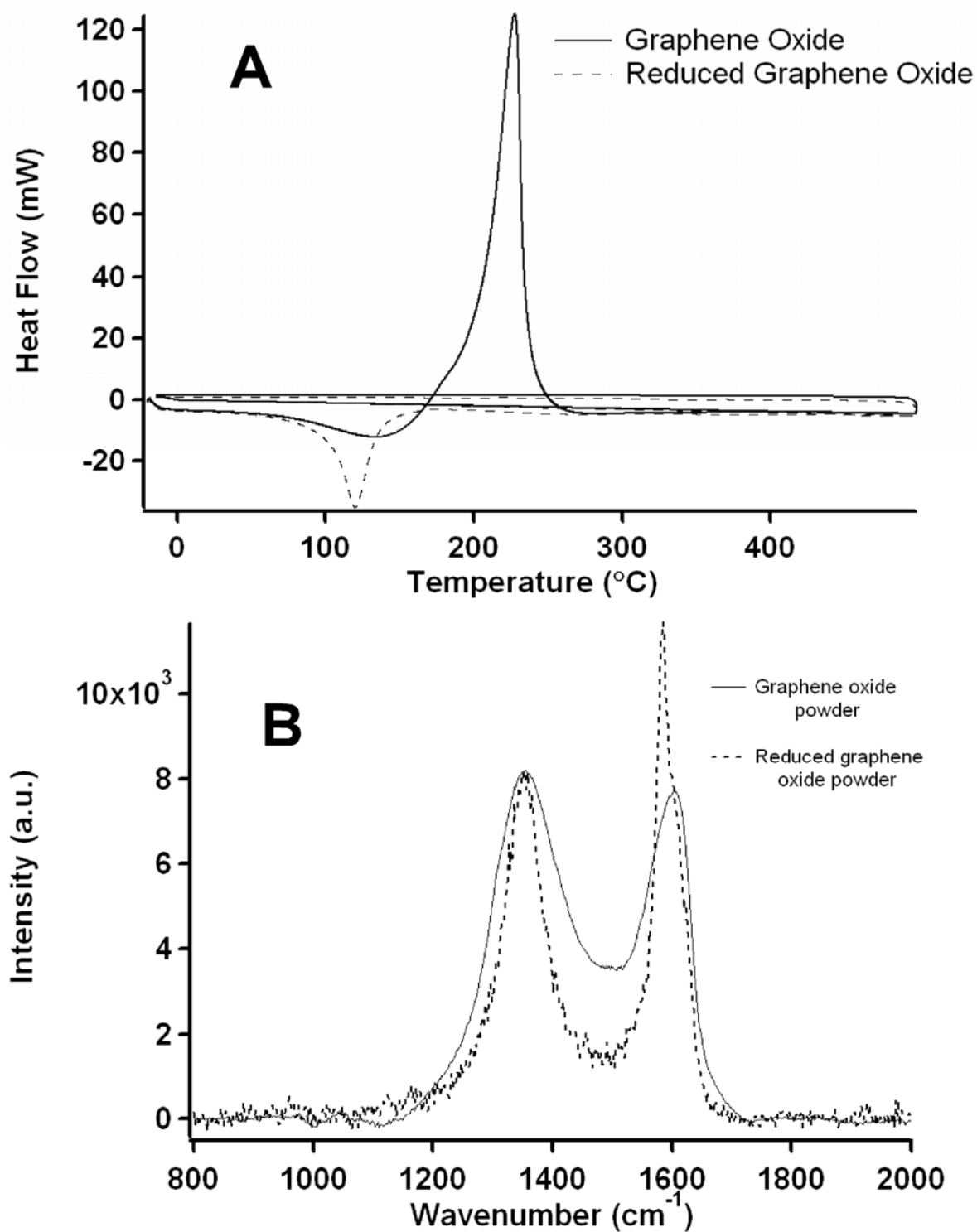


**Figure 2.** A) DSC curves of graphene oxide and reduced graphene oxide powders; B) Raman spectra of the same two samples.

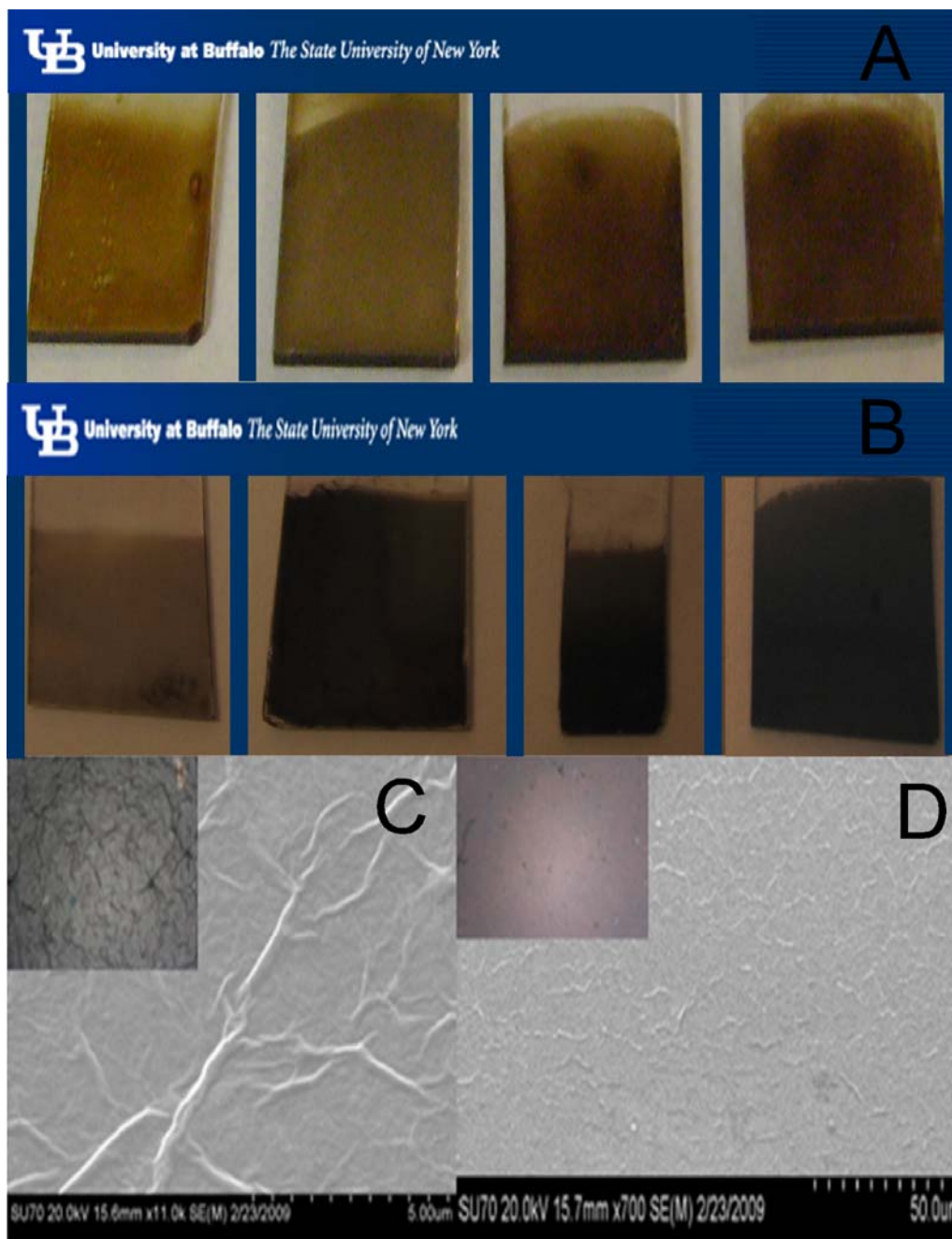


**Figure 3.** A) Digital photographs of graphene oxide films; B) Digital photographs of KOH/hydrazine-reduced graphene films, the film thicknesses obtained from spectroscopic ellipsometry for these films are: (from left to right)  $9.6 \pm 0.2$  nm,  $84.2 \pm 1.1$  nm,  $108.6 \pm 0.9$  nm, and  $146.3 \pm 1.6$  nm; C) SEM image of a KOH/hydrazine-reduced graphene film; D) SEM image of a graphene oxide film. The insets show optical microscopy images.

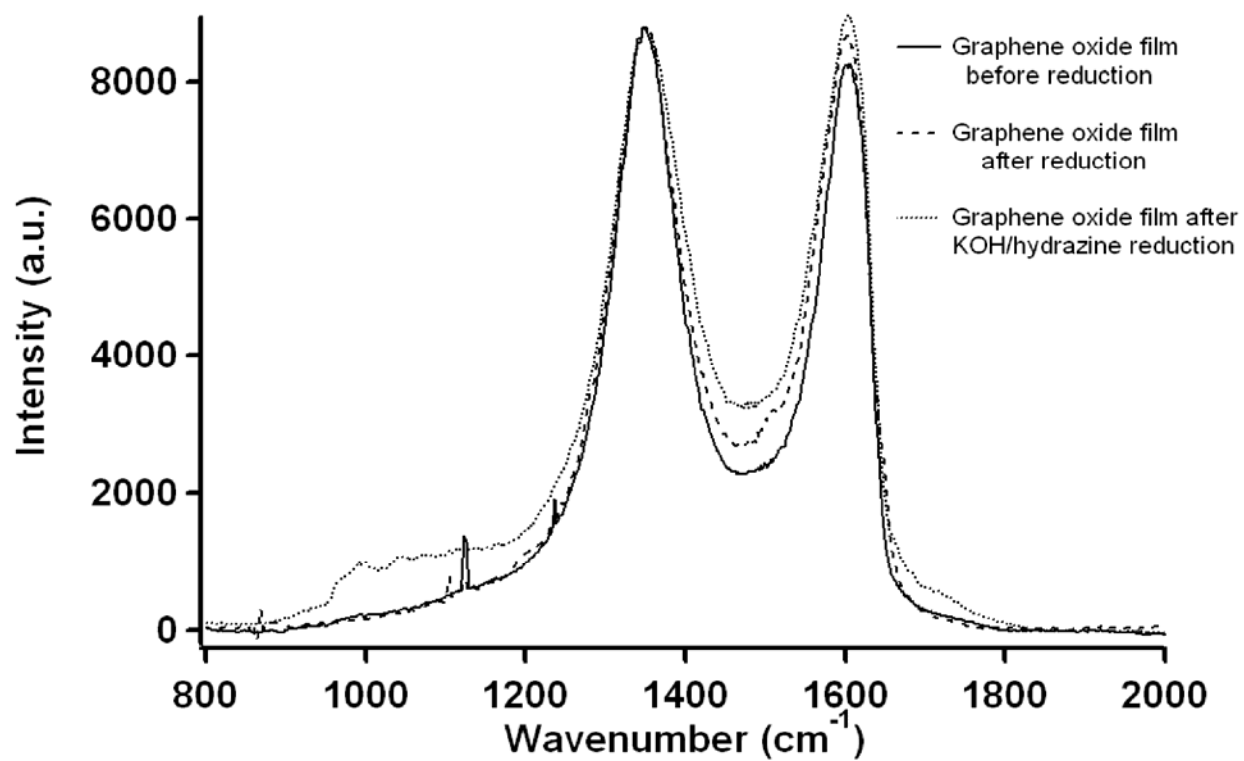


**Figure 4.** Raman spectra for three distinct films: an as-deposited graphene oxide film; the same film after reduction by dip-coating in an aqueous solution of hydrazine; and an as-deposited KOH/hydrazine reduced graphene oxide film.

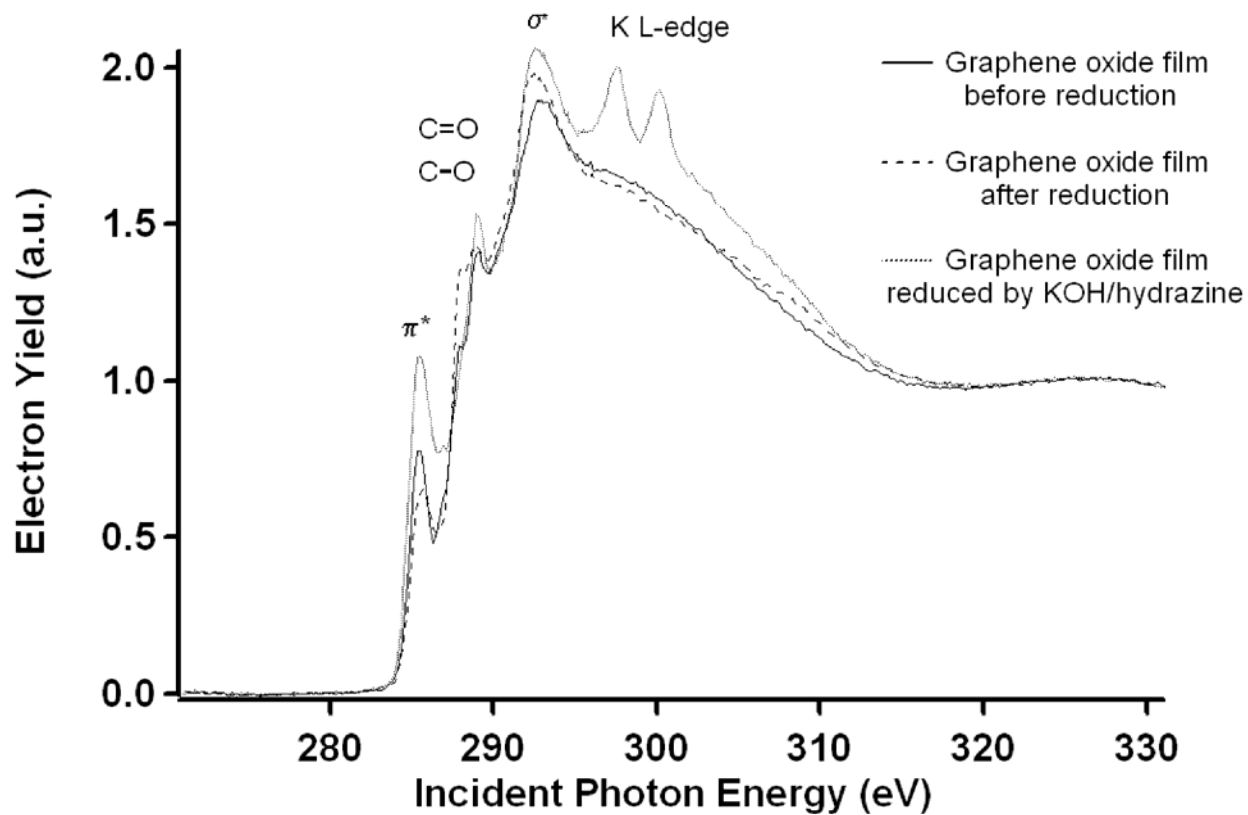


**Figure 5.** Magic angle ( $54.7^\circ$  incidence) C K-Edge NEXAFS spectra for three separate films: an as-deposited graphene oxide film; the same film after reduction by dip-coating in an aqueous solution of hydrazine; and an as-deposited KOH/hydrazine-reduced graphene film.

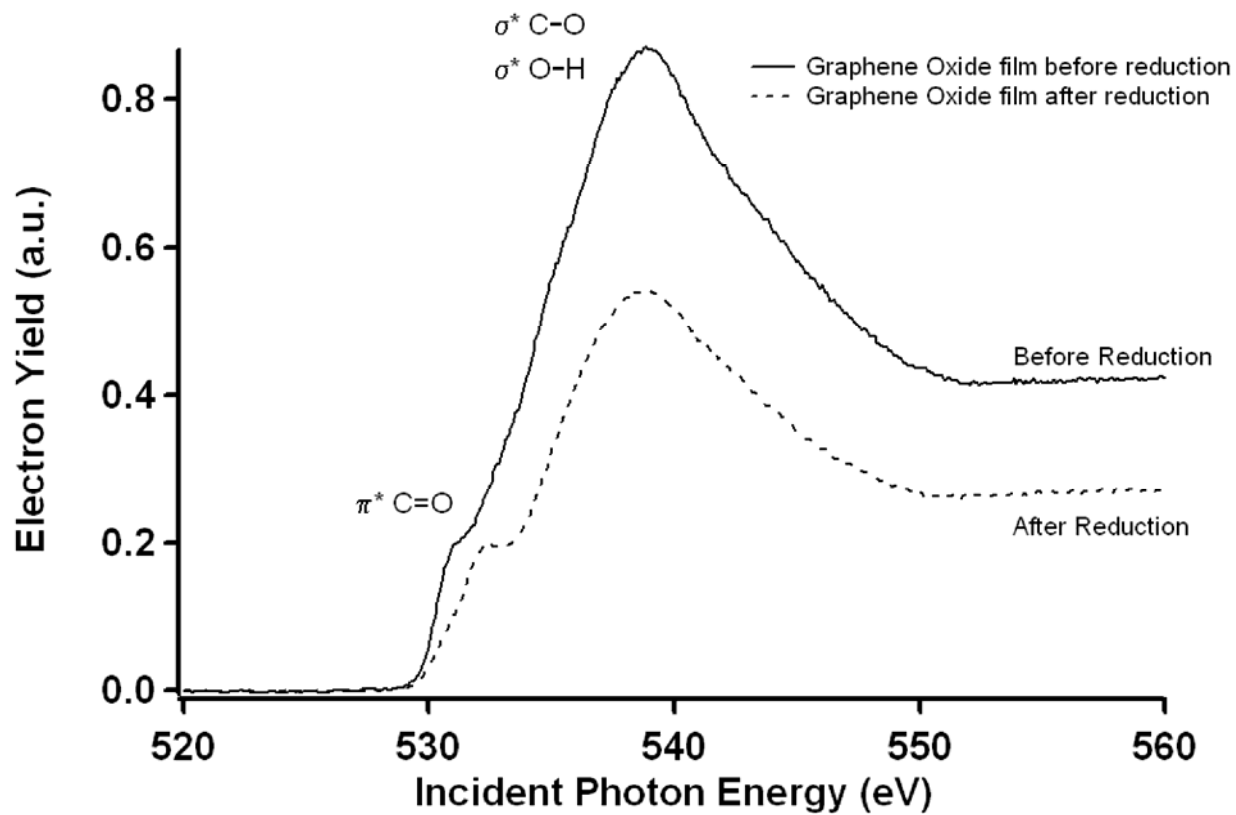


**Figure 6.** Magic angle O K-edge NEXAFS spectra for an as-deposited graphene oxide film and the same film after reduction by dip-coating in an aqueous solution of hydrazine.

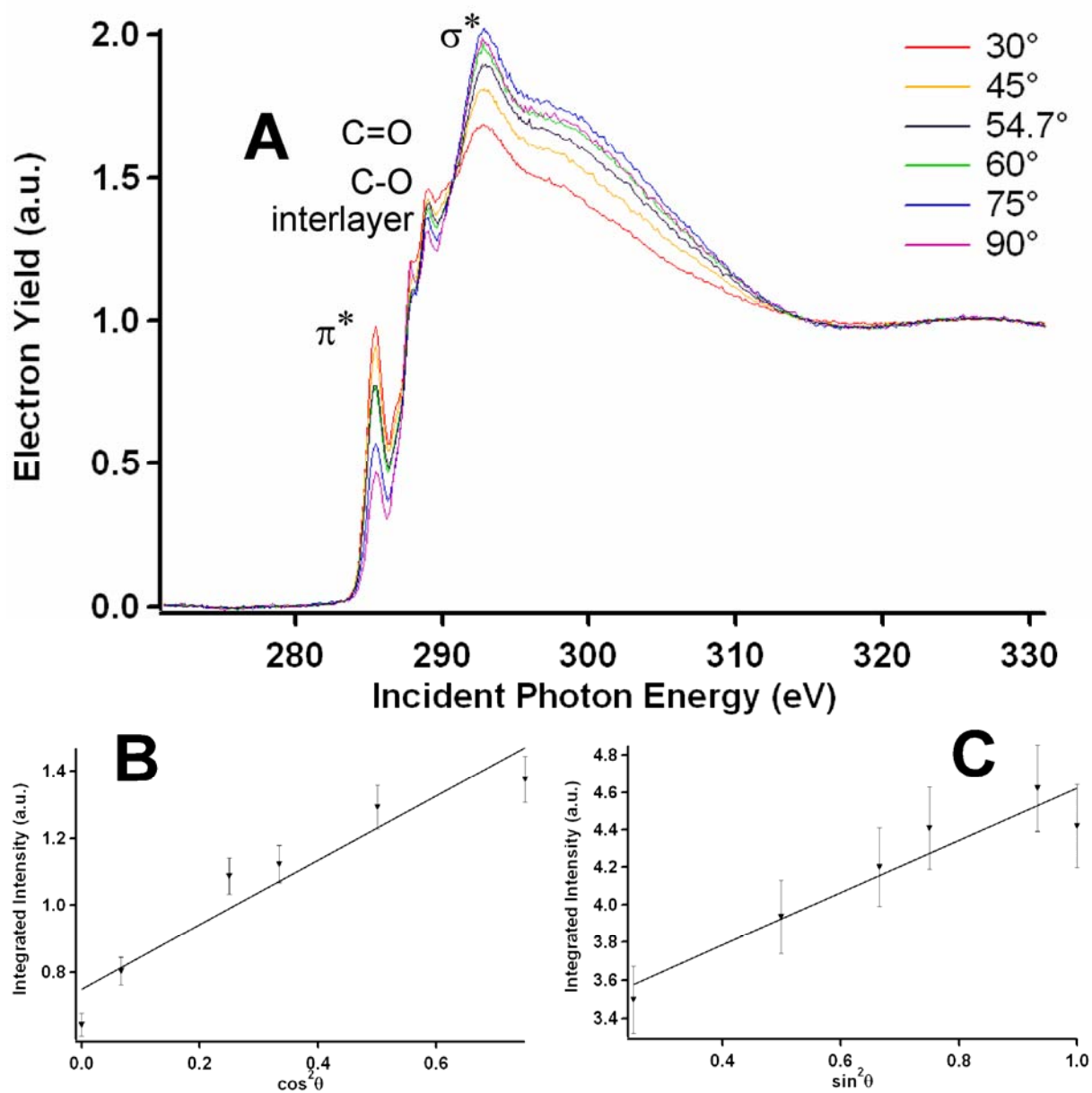


**Figure 7.** A) Polarized C K-edge spectra for an as-deposited graphene oxide film before hydrazine treatment; all spectra have been pre- and post-edge normalized; B) Integrated intensity of the  $\pi^*$  resonance versus the angle of incidence; the solid line shows the  $\cos^2\theta$  dependence of the  $\pi^*$  intensities; C) Integrated intensity of the  $\sigma^*$  resonance versus the angle of incidence; the solid line shows the  $\sin^2\theta$  dependence of the  $\sigma^*$  intensities.

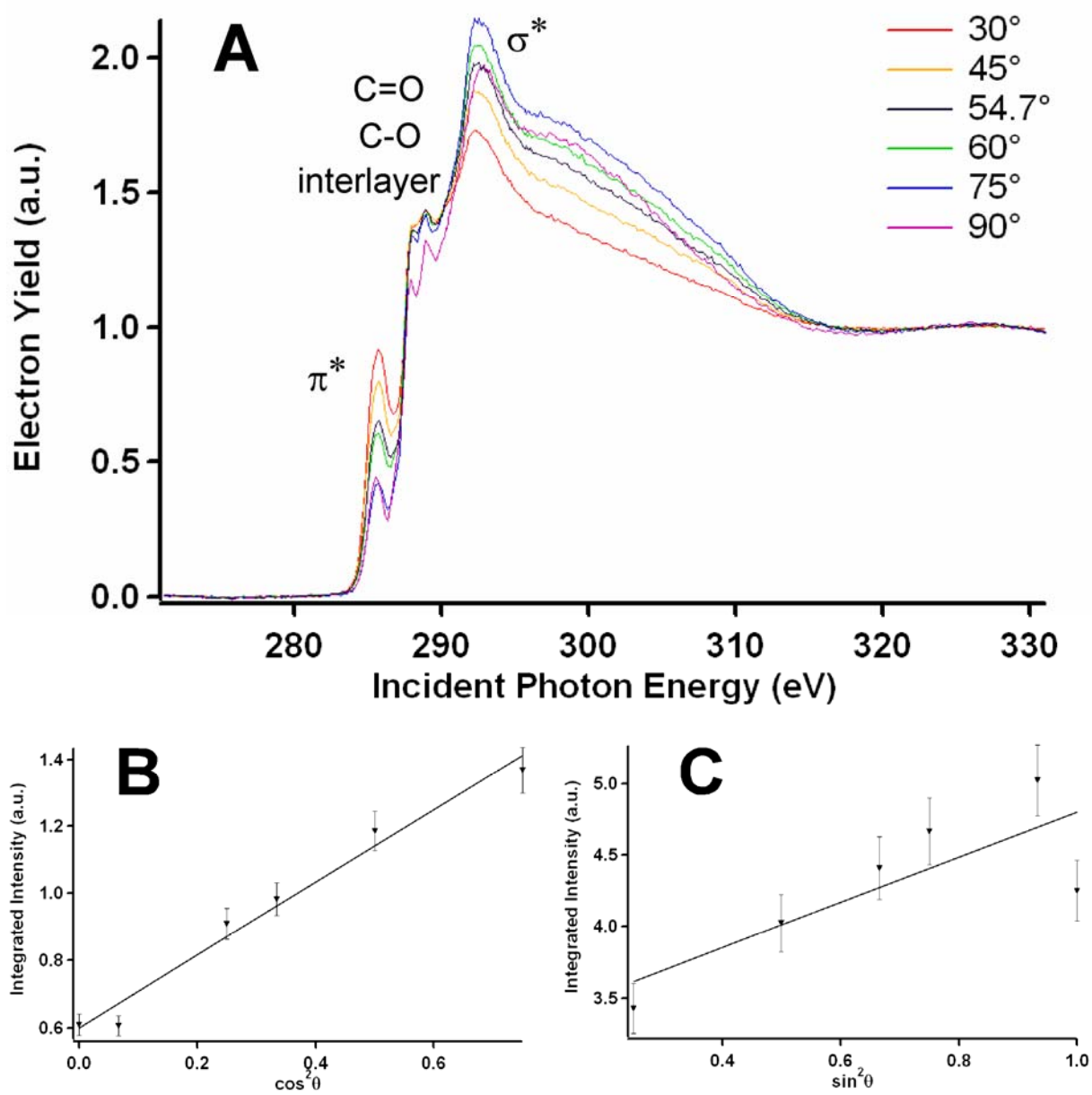


**Figure 8.** A) Polarized C K-edge spectra for an as-deposited graphene oxide film after hydrazine treatment; B) Integrated intensity of the  $\pi^*$  resonance versus the angle of incidence; the solid line shows the  $\cos^2\theta$  dependence of the  $\pi^*$  intensities; C) Integrated intensity of the  $\sigma^*$  resonance versus the angle of incidence; the solid line shows the  $\sin^2\theta$  dependence of the  $\sigma^*$  intensities.

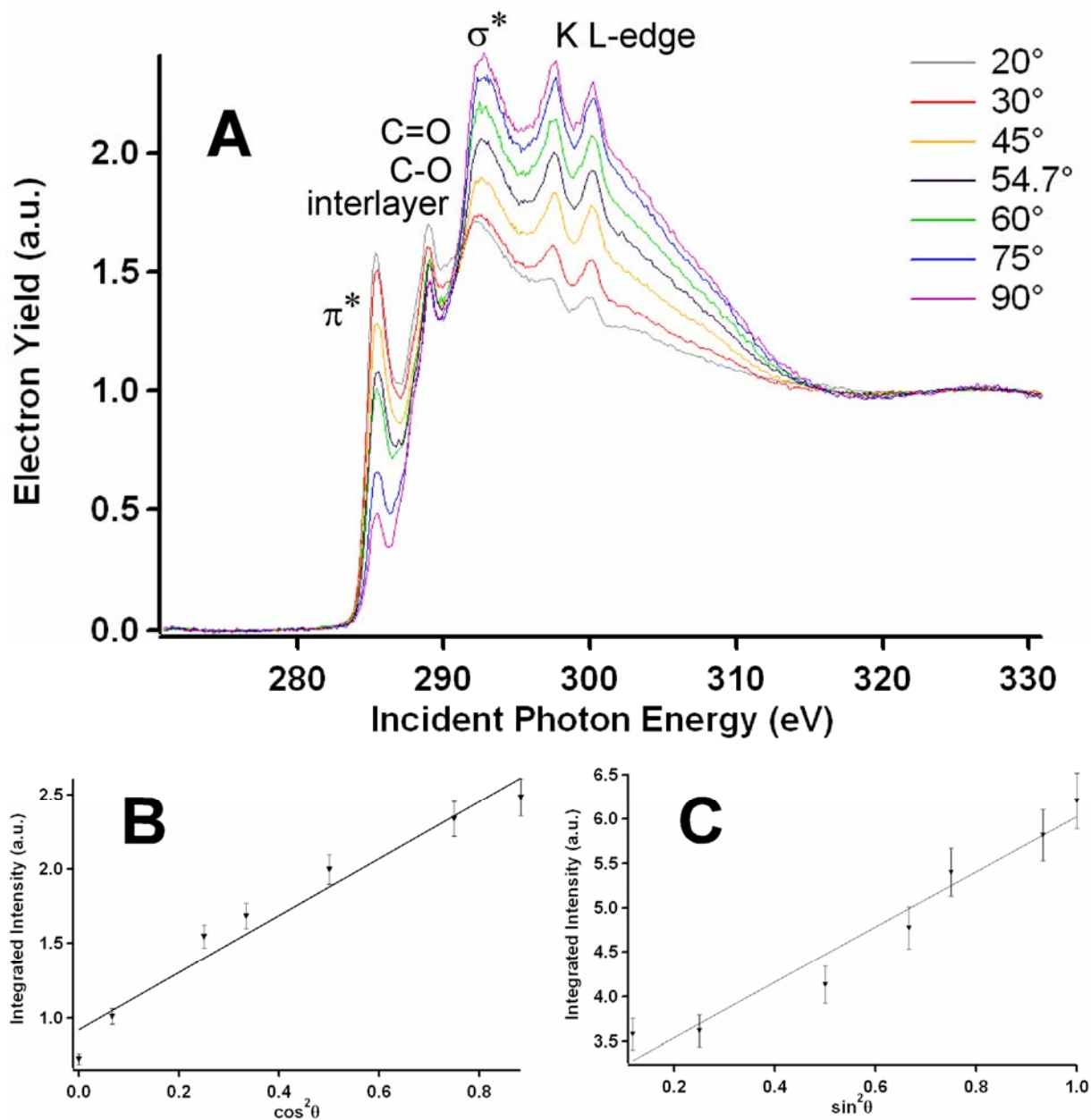


**Figure 9.** A) Polarized C K-edge spectra for an as-deposited KOH/hydrazine reduced graphene film; B) Integrated intensity of the  $\pi^*$  resonance versus the angle of incidence; C) Integrated intensity of the  $\sigma^*$  resonance versus the angle of incidence; the solid line shows the  $\sin^2\theta$  dependence of the  $\sigma^*$  intensities.

Film Type	Dichroic Ratio
KOH/hydrazine reduced film	$-0.59 \pm 0.08$
Graphene oxide before hydrazine reduction	$-0.45 \pm 0.08$
Graphene oxide after hydrazine reduction	$-0.47 \pm 0.08$

**Table 1.** Dichroic ratio calculated from the polarized NEXAFS spectra for three separate films (Equation 1): an as-deposited graphene oxide film; the same film after reduction by dip-coating in an aqueous solution of hydrazine; and an as-deposited KOH/hydrazine-reduced graphene film.